Lead Article

Acta Cryst. (1992). B48, 553–572

Chemical and Steric Constraints in Inorganic Solids*

BY I. D. BROWN

Institute for Materials Research, McMaster University, Hamilton, Ontario, Canada L8S 4M1

(*Received* 14 *December* 1991; *accepted* 21 *February* 1992)

Abstract

The structures observed for many inorganic solids are the result of a compromise between the conflicting requirements of chemical bonding and three-dimensional geometry. The ideal chemical structure and bond geometry can be predicted using the bond-valence model which is developed in some detail. The constraints imposed on this geometry when the ideal structure is mapped into three-dimensional space require, in many cases, that ideal bond lengths be strained. Particularly in compounds containing bonds of intermediate strength (*e.g.* the oxides and halides of di- and trivalent cations), the relaxation of this strain can result in non-stoichiometry, stabilization of unusual oxidation states, distortion of bonding environments and lowering of symmetry. The resulting rich crystal chemistry is often associated with important physical properties such as ferroelectricity and superconductivity. Examples are given which show that these properties can, at least in some cases, be derived directly from the chemical formula by considering the problems of generating a structure that conforms to both the chemical and the spatial constraints.

1. Introduction

Although the coordination environment of most cations in inorganic solids is isotropic, the environment found around Cu^{2+} is almost always tetragonally distorted with two long and four short bonds. This distortion is generally attributed to an electronic effect arising from the presence of nine *d* electrons in the valence shell. The observation of a similar distortion around Ni in La_2NiO_4 by Müller-Buschbaum & Lehmann (1978) was a puzzle since the environment of Ni^{2+}, with only eight *d* electrons, was expected to be isotropic.†

Since 1978 the structures of both La_2NiO_4 and the isostructural La_2CuO_4 have been extensively studied, and the distortion around Ni is now understood to be related primarily to steric effects arising from the geometric constraints that force some of the Ni—O bonds to be compressed and some of the La—O bonds to be stretched. It is the intent of this paper to explore the interplay between chemical and steric requirements in the formation of inorganic solids, requirements which, under suitable conditions, can stabilize unlikely stoichiometries and oxidation states, and result in unusual physical properties such as ferroelectricity and superconductivity.

The fact that we find it necessary to explain the distortions in La_2CuO_4 and La_2NiO_4 implies that there is a norm (regular octahedral coordination) that we would otherwise expect for the environment of Cu or Ni. It is one of the striking observations of inorganic structural chemistry that most cations do have regular, or near regular, coordination spheres and we only find it necessary to explain deviations from this regularity. The model used in this paper starts with the premise that both cation and anion coordination spheres should be as regular as possible (see §3.2). This premise leads to the prediction of a set of 'ideal bond lengths' for a given compound. The deviations from these ideal lengths, which we recognize as distortions, can be ascribed either to electronic effects (*i.e.* electronic anisotropies, as in the case of Cu^{2+}) or to steric effects (as in the case of Ni^{2+} described above).‡

Since electronic distortions cannot yet be quantitatively predicted, the main focus of the paper will be on the influence of steric effects.

To understand how steric effects can influence the chemistry of a solid, one needs a model that can predict the ideal bonding geometry, that is, the geometry that would be expected if steric and electronic effects were not present. The traditional approach to modelling inorganic structure is to place

* *Editorial note*: This invited paper is one of a series of comprehensive Lead Articles which the Editors invite from time to time on subjects considered to be timely for such treatment.

† This is true for high-spin Ni, the form usually found in oxides. Low-spin Ni does show the Jahn–Teller distortion, but usually in the extreme form of square-planar coordination.

‡ In practice, electronic and steric effects contribute to the distortions in both compounds, but only the Cu compound has a strong enough electronic anisotropy to produce a distortion in the absence of steric stress.

0108-7681/92/050553-20$06.00

the atoms in a three-dimensional array and move them to positions that minimize the total energy. Since the only configurations accessible in this model are those which already exist in three-dimensional space, any steric constraints are necessarily built into the model and cannot be separated out. This approach, while it often yields good predictions of structure and physical properties, cannot be used to show how steric strain produces the variety of interesting properties that are observed. For this purpose a different model is needed.

Such a model does exist, and is widely used, in organic chemistry. In the chemical-bond model, the chemical formula of a molecule is first transformed into a 'two-dimensional' structure diagram, or bond graph, which represents the molecule schematically by a series of bonds connecting the different atoms. This graph is then mapped into Euclidian space to obtain the three-dimensional structure or conformation. The mapping itself involves two steps. In the first, ideal bond distances and angles are predicted from the two-dimensional graph, using a knowledge of the lengths of double and single bonds, modified by the known effects of the various substituent groups in the molecule. In the second step, this ideal geometry is mapped into three dimensions. The mapping is generally not unique, several conformations are possible, but the range of conformers is limited by steric effects. Combinations of torsion angles that would cause different parts of the molecule to overlap are forbidden. In the extreme case of a highly overcrowded molecule, a three-dimensional mapping may not be possible unless the ideal geometry is strained. Strained molecules are less stable and for this reason only those with small strains are expected to exist. The low stability of strained molecules is a factor that must be taken into account in planning a chemical synthesis.

The chemical-bond model used in organic chemistry does not carry over directly into inorganic chemistry, but a version of it, the bond-valence model, described in §3, does give good predictions of the bonding geometry of those inorganic compounds that do not show steric strain. This model has its roots in Pauling's (1929) concept of bond strength, but it has recently been developed into a simple predictive model that provides insight into the interactions between chemistry and spatial constraint. As with the chemical-bond model, the bonding geometry is predicted from a two-dimensional bond graph (see for example Fig. 13*a*) though using different rules. In particular, the bonds are not restricted to integral bond orders, but can have any strength (bond valence) between 0 and 2, or even higher. The mapping into three-dimensional space is also more complex, since the structures are infinitely connected and usually show translational symmetry, placing severe constraints on the permitted conformations. It is not surprising, therefore, that steric effects play a more important role in inorganic chemistry than they do in organic chemistry.

The importance of steric effects in a given structure depends on the strength of the bonds. For strong bonds, those with valences (or strengths) greater than 1.0 valence units (v.u.), the structure adopts the ideal chemical geometry. These bonds are stiff and cannot be adapted to the steric constraints. If the structure cannot be mapped into three-dimensional space without strain, it will not exist. This is the regime of complex anions such as sulfates and phosphates, of many of the silicates and of most organic molecules. At the other extreme, bonds with valences less than 0.2 v.u., exemplified by bonds to the alkali metals, are soft and their lengths readily adapt to the spatial requirements. In between these two regimes is a regime in which both the chemically ideal geometry and the steric constraints are equally important. The bonds can be strained, but the strain energy is relatively large. Compounds in this regime attempt to reduce the stress associated with this strain by changing either the lengths of their bonds, their compositions or the oxidation states of their atoms. These are the oxides and halides of di- and trivalent cations, the compounds that show the widest range of structures and properties. It is here that the bond-valence model provides chemical insights into an unexpectedly rich field of crystal chemistry.

2. Theories and models of inorganic structure

2.1. *Introduction*

Before giving an account of the bond-valence model, it is useful to review some of the traditional approaches to bonding in inorganic solids.

The nineteenth century approach to structural chemistry was strictly empirical. As late as 1900, there was no independent evidence for the existence of either of its two key concepts, the 'atom' or the 'chemical bond'. In the early years of this century, physicists discovered the atom and developed a physical theory, quantum mechanics, with which to describe its properties. Despite the enormous success of quantum mechanics in atomic and subatomic physics, its application to chemistry has been thwarted by computational complexities. Surprisingly, even in cases where it has been used, it has not led naturally to the concept of a chemical bond. There is still no quantum-mechanical explanation for why, in many cases, one can ignore all the interactions between atoms except for those between certain nearest neighbours.

Consequently, two separate threads run through the twentieth-century theory of chemical structure: one, using the rigorous physical theory, is frustrated by the complexities of real chemical systems, the other, developed from the empirical nineteenth-century bond model, lacks physical justification. Even though both models have been successfully used to describe organic molecules, neither has until recently been effective in describing inorganic materials. Therefore, a third approach, the ionic or two-body-potential model, was developed. This model treats inorganic compounds as composed of ions, whose cohesion is provided by Coulomb forces, but whose spatial arrangement is determined by the repulsions that occur between atoms in contact.

For a long time none of these models provided quantitative prediction of inorganic structure but, in recent years, both the ionic model and the bond model (in the form of the bond-valence model) have become usefully predictive. The bond-valence model is the focus of the present article and will be developed in §3, but a few comments on the quantum-mechanical and ionic models are appropriate.

2.2. *Quantum mechanics*

Attempts to apply quantum mechanics to inorganic solids have been hindered by the practical difficulties of solving the Hamiltonian for infinite structures. Most quantum-mechanical calculations in inorganic chemistry have been confined to the study of small atomic clusters which are then used as models for the same cluster in the solid. Quantum-mechanical calculations are useful for interpreting the local environment of an atom, but they are less useful for predicting the way in which these local environments are combined to create a complex crystal structure. In particular they cannot shed light on the strains introduced by translational symmetry. In spite of these limitations, Bader (1990) has shown how atom fragments and bond paths can be uniquely identified in the topology of the electron density, and has shown, using catastrophe theory, that there is a physical basis for the changes that occur in the bond graph during a chemical reaction. Although his calculations have so far been confined to finite clusters, they suggest that there is a physical basis for the bond model.

2.3. *The ionic model*

In its simplest form the ionic model treats the atoms as hard charged spheres held together by Coulomb forces. More sophisticated versions treat the atoms as soft spheres by using a two-body potential that incorporates both an attractive Coulomb term and a short-range repulsive term. Two simple forms of this potential have been proposed by Born and his coworkers [Born & Landé (1918), equation (1); Born & Mayer (1932), equation (2)].

$$U_{ij} = A\frac{q_i q_j}{R_{ij}} + \frac{B}{R_{ij}^n} \tag{1}$$

$$U_{ij} = A\frac{q_i q_j}{R_{ij}} + C\exp\left(-\frac{R_{ij}}{D}\right) \tag{2}$$

The first term in both expressions is a Coulomb potential in which A is a dimensional constant, q_i and q_j are the physical charges on the two atoms (usually taken to be the same as the formal ionic charge) and R_{ij} is the interatomic distance. This term may be attractive or repulsive, but the net effect of summing this term over all pairs of atoms in the crystal (the Madelung energy) is attractive. The summation does not converge quickly but various efficient methods are available for its evaluation (Ewald, 1921; Bertaut 1952). Hoppe (1975) has shown that, in complex crystals, the contribution of a particular cation to the Madelung energy (MAPLE, the MAdelung Part of the Lattice Energy) is invariant from one compound to another and he has used MAPLE calculations to test the correctness of new structure determinations. O'Keeffe (1990) has shown that the Madelung potential of a site scales as the oxidation state of the atom that occupies it.

The second term in both equations represents the repulsion between adjacent atoms resulting from the overlap of their electron clouds. More elaborate functions than those shown in (1) and (2) are possible but the simplicity of these forms, each of which involves only two fitted parameters for each type of interaction, has made them popular. The exponential form (2) is physically more realistic (Pauling, 1927) but the power law (1) is computationally simpler. Various methods have been proposed for choosing the repulsion parameters (B and n, or C and D in the above equations), ranging from fitting them to the observed elastic constants, to fitting them to the potential calculated from an *ab initio* treatment of the two isolated atoms (*cf.* Catlow, 1977; Catlow, Thomas, Parker & Jefferson 1982; Burnham 1990; Kramer, Farragher, Van Beest, Van Santen, 1991). These potentials are not always transferable between different compounds and sometimes corrections are needed for the polarization of the atoms, but, when used carefully, the ionic model can give good predictions for the structure and physical properties of inorganic materials, even those in which the bonding is clearly not ionic. However, the model does not allow an explicit treatment of the steric strain because it starts with the atoms already occupying positions in three-dimensional space and so cannot be used to determine the ideal bond lengths.

3. The bond-valence model

3.1. *Introduction*

Although the concept of a bond does not occur directly in either the quantum mechanical or the ionic model, the term 'bond' is often used in the description of inorganic structures by analogy with its use in organic chemistry. Most chemists would use the term to describe the interactions between S and its neighbouring O atoms in the sulfate ion, SO_4^{2-}, but would be more reluctant to use it to describe the interaction between Na and Cl in NaCl. In these contexts it is used descriptively and a precise definition is not necessary.

If bonds are to be used as the basis for a chemical model, their properties have to be clearly defined. The first step was taken in 1929 when Pauling introduced the idea of the strength of a bond in the second of his five 'principles determining the structure of complex ionic crystals':

> 'In a stable coordination structure the electric charge of each anion tends to compensate the strength of the electrostatic valence bonds reaching it from the cations at the centers of the polyhedra of which it forms a corner; that is, for each anion
>
> $$V_j = \sum_i V_i/N_i = \sum_i s_i.$$'

Here V_j is the anion valence (formal oxidation state), V_i the cation valence, N_i the cation coordination number and s_i is often referred to as the 'Pauling bond strength' of the cation.

With the accumulation of accurate bond geometries for a large number of compounds, it was possible to demonstrate that Pauling's second rule was better obeyed if the relationship between the strength and the length of a bond was taken into account (Byström & Wilhelmi, 1951; Zachariasen, 1954). Donnay & Allman (1970) were able to generalize Pauling's 'bond strength' into 'bond valence', a property that correlated inversely with bond length. The implications of linking Pauling's second rule to the bond geometry are the subject of the rest of this section and are developed within a formal and rigorous model.

3.2. *Basic assumptions*

The bond-valence model is based on the following assumptions:

(1) Any chemical structure can be considered as a network in which the nodes are atoms and the edges are bonds. This expresses the conventional chemical picture of a solid in terms of a bond diagram or graph and applies equally to organic and inorganic compounds. Examples are shown in Figs. 11(*a*) and 13(*a*).

(2) Atoms are characterized by three properties: atomic number (Z, defining the chemical element), valence (V, defining the oxidation state) and electronegativity (χ). V is usually (but not necessarily) an integer and obeys the rule that the sum of all atomic valences in the crystal is zero. It is determined, in part, by the column in the periodic table in which the atom lies and can be thought of as the number of electrons that the atom contributes to chemical bonding. χ is a number related to the Lewis acid strength defined in §3.5.2. V may be positive or negative. Atoms with positive valence are called *cations*, those with negative valence are called *anions*. These are labels of convenience. There is nothing in the bond-valence model that implies the physical nature of the bonding. In §3.8 it is shown that the bond-valence model is consistent with both ionic and covalent views of bonding.

(3) Bonds occur only between neighbouring atoms whose valences have opposite sign. This restricts the model to the acid–base bonds typically found in inorganic materials. A bond network with this property is said to have a *bipartite graph* in which all closed paths in the graph have an even number of bonds (edges). The graph is also *directed*, since the bonds are assumed to be directed from the anions to the cations. Although this assumption appears to be quite restrictive, it is obeyed by the majority of inorganic compounds and, in any case, §3.3 shows that a non-bipartite bond graph can often be converted into bipartite one.

(4) Bonds are characterized by their bond valences (s) and their bond lengths (R). Bond valence is rigorously defined in assumption (5) below, but it is qualitatively the same as bond strength or bond number and can be thought of as the number of electron pairs that are associated with the bond. *Bond length* is defined as the distance between atomic nuclei which, for most atoms, lie at the centers of their electron cores.

(5) *Bond valences* (s) are related to atomic valences (V) through the two network equations:

$$\sum_j s_{ij} = V_i \tag{3}$$

$$\sum_{\text{loop}} s_{ij} = 0 \tag{4}$$

where the subscripts i and j refer to different atoms. These equations, which are similar to the Kirchhoff equations used to solve electrical networks, uniquely define the bond valences for a given graph. There are several approaches to solving these equations which will not be discussed here. Interested readers are referred to papers by Brown (1977), O'Keeffe (1989) and Rutherford (1990).

Equation (3), referred to as the *valence-sum rule*, states that the sum of the bond valences around an atom is equal to its atomic valence. Equation (4),

which states that the sum of the bond valences around any loop (having regard to the direction of the bonds) is zero, is the mathematical condition that results in the most symmetric distribution of atomic valence among the bonds (Brown, 1991*c*). This equation is therefore referred to as the *equal-valence rule*. The two rules together can be summarized by the statement: Each atom shares its valence as equally as possible among the bonds that it forms.

The bond valences predicted by these equations are referred to as *simple bond valences* and give correct predictions of bonding geometry (see §3.4) for the majority of inorganic compounds. Structures in which the bonding is distorted by electronic effects, such as the presence of lone-pair electrons or the Jahn–Teller distortions found around Cu^{2+}, clearly do not obey the equal-valence rule. They are discussed in §3.7. Simple bond valences are referred to as *ideal bond valences* after they have been corrected for electronic effects. Both valence rules may also be violated in the presence of steric constraints as discussed in §4.

3.3. *Structures with non-bipartite graphs*

Assumption (3) restricts the bond-valence model to bipartite graphs, that is, graphs in which bonds are found only between cations and anions. The model runs into inconsistencies if bonds occur between two cations or between two anions. In practice this restriction can be circumvented in a couple of ways. One is to treat the two-bonded cations (*e.g.* Hg_2^{2+}) or anions (*e.g.* O_2^{2-}) as a single node, the only difficulty being how to distribute the atomic valence between the two atoms. An example is given by the trifluoroacetate ion (Fig. 1*a*), whose two C atoms, unlike those in the acetate ion (Fig. 1*b*), are both formally cations and must be treated as a single C_2^{6+} node.

An alternative approach is to split an atom into two nodes of opposite sign, keeping the total valence of the two nodes the same as that of the atom they replace. Thus in $Cu(NO_2)_6^{4-}$ both the Cu and the N bonded to it are formally cations (Fig. 1*c*). The N^{3+} can be split into two nodes, $N1^{a-}$ and $N2^{(3+a)+}$, where a depends on the valence of the fictitious bond between the two nodes N1 and N2 and can have, therefore, any convenient value (Fig. 1*d*). This complex could also have been treated by replacing CuN_6^{20+} by a single node, but useful information about the Cu—N bond would then have been lost.

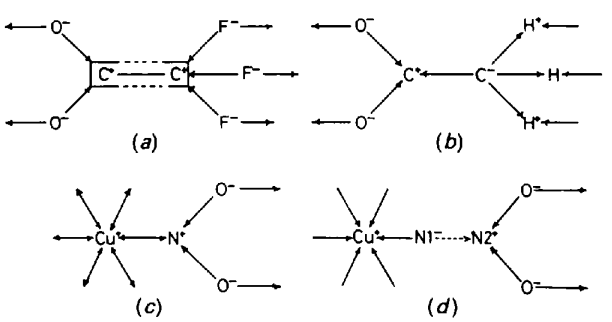

Fig. 1. Examples of the treatment of non-bipartite graphs. (*a*) In the trifluoroacetate ion the two C atoms are treated as a single node. (*b*) The acetate ion has a bipartite graph. (*c*) $Cu(NO_2)_6^{4-}$ ion with cation–cation bonds. (*d*) Treatment of $Cu(NO_2)_6^{4-}$ splitting N into two nodes.

3.4. *Correlation between bond valence and physical properties*

The assumptions of §3.2 lead to a formal description of chemical bonding in terms of atomic valence and simple bond valence, but the usefulness of the description lies in the relationships that exist between bond valences and physical properties. The relationship between bond valence (s) and bond length (R) is particularly well determined, in part because of the large number of accurate measurements of bond length that are available.

The relationship, a typical example of which is given in Fig. 2, is monotonic, and over the small range in which most bonds are found, it can be approximated by either (5) or (6):

$$s_{ij} = \exp\left(\frac{R_0 - R_{ij}}{B}\right), \tag{5}$$

$$s_{ij} = (R_{ij}/R_0)^{-N'}. \tag{6}$$

Here R_0, B and N' are fitted constants, R_0 being the length of a bond of unit valence. Values for these constants have been determined by many workers, by requiring that the values of s_{ij} obey the valence-sum rule (3) in many different compounds. Brown & Altermatt (1985) report values of R_0 for most of the common bonds and have shown that, for most bonds, B can be set equal to 0.37 Å. Brese & O'Keeffe (1991) have extrapolated these results to unknown and less frequently found bonds and they have also shown that the values of R_0 can be expressed as the sum of atomic radii with a small correction that depends on the difference in electronegativity, χ (O'Keeffe & Brese, 1991). An important consequence of the bond-length–bond-valence correlation is that it is possible to predict bond lengths directly from the bond graph using the network equations (3) and (4) together with (5) or (6).

Experimental bond valences, s', can be calculated from observed bond lengths. The sums of experimental valences will not, in general, be exactly equal to the atomic valence and a measure of the discrepancy is given by d_i in (7).

$$d_i = V_i - \sum_j s'_{ij} \tag{7}$$

A convenient measure of the agreement over the whole structure is given by the index, $R1$, which is the root-mean-square average of the d_i values:

$$R1 = \langle d_i^2 \rangle^{1/2}. \quad (8)$$

Experimental uncertainty in the determination of bond lengths can lead to values as large as 0.1 v.u. for these indices, depending on the accuracy of the bond lengths. Larger values of d_i and $R1$ are indicative of strained bonds which can lead to instabilities in the crystal as discussed in §4.

The correlation between bond valence and bond length is well attested, but bond valence also correlates with other bond properties. A correlation with the coefficient of thermal expansion has been demonstrated (Khan, 1976; Hazen & Prewitt, 1977; Bobinski & Ziołkowski, 1991). Force constants and bond energies also increase with bond valence but a quantitative correlation is difficult to determine because there are difficulties in defining, and determining, bond force constants and bond energies (Ziołkowski & Dziembaj, 1985).

3.5. *Some theorems*

3.5.1. *The distortion theorem.* The presence of strain in a structure can lead to a distorted cation environment as shown by the corollaries to the following theorem.

Any deviation of the valences of the bonds formed by an atom from their average valence will increase the average valence providing the average bond length remains constant.

An alternative statement is:

Any deviation of the lengths of the bonds formed by an atom from their average length will increase the average length providing the average bond valence remains constant.

This theorem derives from the concave shape of the bond-valence–bond-length correlation (see Fig. 2). Increasing the valence of one O—H bond and decreasing the valence of the other by the same amount increases the longer bond by more than it decreases the shorter, thus increasing the average bond length. This theorem has three important corollaries: (1) If an atom is placed in a cavity that is too large, so that the average length of its bonds is too long to satisfy the valence-sum rule, the valence sum can be increased by making some bonds longer and others shorter, *e.g.*, by allowing the atom to move off center within the cavity. Where such a distortion occurs, the equal-valence rule is clearly not obeyed, but the extent of the deviation can be predicted if the cavity size is known. (2) Since the application of hydrostatic pressure reduces the average bond length, pressure will tend to make distorted atomic environments more symmetric. Pressure has the effect of reducing the space available to an atom and so, for a given atom, will remove distortions. (3) Since a symmetric coordination environment can be thought of as a highly distorted form of an environment with a higher coordination number, pressure will stabilize higher coordination numbers. An example is provided by the pressure-induced phase transition of the alkali halide crystals from the NaCl to the CsCl structure. The increase in coordination number from six to eight provides relief from the

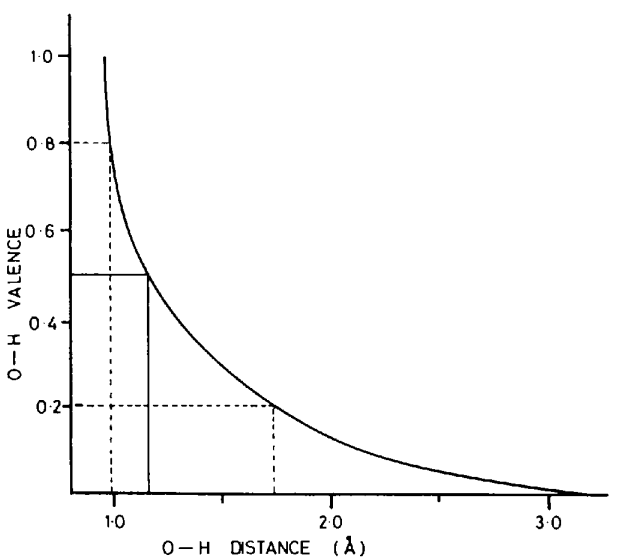

Fig. 2. Bond valence as a function of bond length for bonds between H and O [reprinted with permission from Brown (1989), © 1989 American Chemical Society].

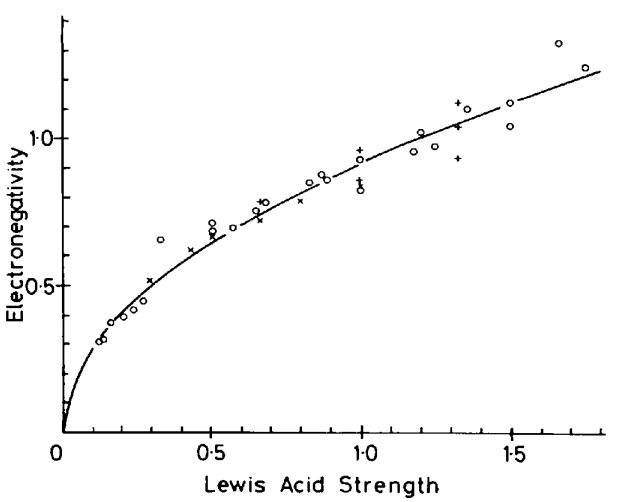

Fig. 3. Correlation between electronegativity and Lewis acid strength [reprinted with permission from Brown & Skowron (1990), © 1990 American Chemical Society]. Circles are main-group elements in their highest oxidation state. + and × are the same elements in lower oxidation states.

stress. The average of the shortest 6 + 2 distances of the NaCl structure is larger than the average of the eight shortest distances of the CsCl structure, even though the eight bonds of the CsCl form are longer than the six shortest distances of the NaCl form.

3.5.2. *The valence-matching principle.* Stable compounds will tend to form only between cations whose Lewis acid strength is approximately equal to the Lewis base strength of the anion. This theorem follows directly from the definition of *Lewis acid strength* as the expectation value of the valence of a bond formed by a cation, and of the *Lewis base strength* as the expectation value of the valence of a bond formed by an anion. Since the same bond links the two, the expectation values should be similar.

The Lewis acid strength is determined by noting that coordination number (n) is a characteristic property of cations, particularly those in high oxidation states. Representing the characteristic coordination number by the average coordination number, $\langle n \rangle$, found in a large number of stable solids, we can use the valence-sum rule to calculate the average valence, $\langle s \rangle$, of the bonds formed by a given cation as shown in (9) (Brown, 1988*b*).

$$\langle s \rangle = V/\langle n \rangle \qquad (9)$$

According to the equal-valence rule, $\langle s \rangle$ will be close to the actual valence of each of the bonds formed by the cation. The average valence of a cation, $\langle s \rangle$, is then the Lewis acid strength, S_a (10), so called because it correlates with electronegativity (Fig. 3) (Brown & Skowron, 1990).

$$S_a = \langle s \rangle = V/\langle n \rangle, \quad V > 0 \qquad (10)$$

Values of the Lewis acid strengths of some common cations are given in Table 1.

A corresponding equation, (11), can be used to define a Lewis base strength or the expectation value of the bond valence, S_b, for anions (Table 2).

$$S_b = \langle s \rangle = V/\langle n \rangle, \quad V < 0 \qquad (11)$$

For complex oxyanions, $\langle n \rangle$ can be approximated by assuming that terminal O atoms are four-coordinate and bridging O atoms are three-coordinate. In practice anions form bonds with a wider range of valences than cations. It is therefore convenient to call S_b the *normal Lewis base strength* and to define a *maximum base strength*, S_m, according to (12) where

$$S_m = V/n_{\min} \qquad (12)$$

and $n_{\min}$ is the smallest possible coordination number of the O atom, normally 2 but occasionally 1 or 3. The calculation of the normal and maximum base strength of water is illustrated in Fig. 4.

The valence-matching principle is illustrated by Dent-Glasser's (1979) observation that the alkali metals tend not to form orthosilicates, and transition metals tend not to form highly polymerized silicates. Fig. 5 shows that the low base strength of the polymerized silicate ions matches well the low acid strength of the alkali metals, whereas the more strongly acid transition metals bond readily to the more strongly basic orthosilicate ion. The compounds that are not observed are those that are poorly matched.

Hawthorne (1985) has developed this idea to model the geogenesis of minerals in rocks. He assumes that the silicate framework that forms is the one whose Lewis base strength best matches the acid strengths of the available cations.

Table 1. *Some Lewis acid strengths (from Brown, 1988b)*

Li	Be	B	C	N	O	F
0.205	0.501	0.87	1.35	1.67		
Na	Mg	Al	Si	P	S	Cl
0.156	0.334	0.57	1.00	1.25	1.5	1.75
K	Ca	Ga	Ge	As	Se	Br
0.126	0.274	0.65	0.89	1.13	1.5	
Rb	Sr	In	Sn	Sb	Te	I
0.120	0.233	0.50	0.68	0.83	1.20	1.2
Cs	Ba	Tl	Pb	Bi^{3+}		
0.113	0.195	0.49	0.70	0.48		
Sc^{3+}	Ti^{4+}	V^{5+}	Cr^{6+}	Mn^{3+}	Fe^{3+}	Co^{3+}
0.49	0.67	1.08	1.50	0.52	0.53	0.51
	Mn^{2+}	Fe^{2+}	Co^{2+}	Ni^{2+}	Cu^{2+}	Zn^{2+}
	0.34	0.34	0.35	0.34	0.39	0.40

Table 2. *Some Lewis base strengths*

S_b	S_m	Anion
0.50	2.00	O^{2-}
0.33	1.00	SiO_4^{4-}, BO_3^{3-}
0.25	0.75	PO_4^{3-}
0.22	0.67	CO_3^{2-}, HPO_4^{2-}
0.21	1.00	F^-
0.17	0.50	SO_4^{2-}, Cl^-, $H_2PO_4^-$
0.17	0.34	H_2O
0.11	0.33	NO_3^-
0.09	0.50	Br^-
0.08	0.25	ClO_4^-, BF_4^-
0.06	0.50	I^-

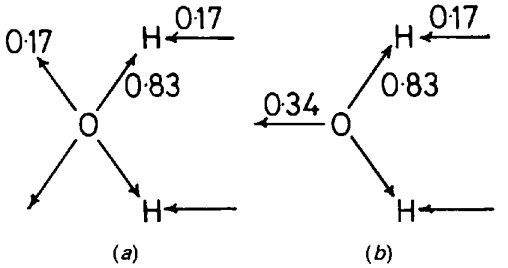

Fig. 4. The base strength of water. (*a*) The normal Lewis base strength is 0.17 v.u. (*b*) The maximum Lewis base strength is 0.34 v.u.

3.6. *A useful technique – the valence-sum map*

A special valence technique was developed by Waltersson (1978) in order to locate the Li atoms in lithium tungstates. He calculated the valence sum that a Li atom would have if placed at any arbitrary point in the crystal. Any position where this value is 1.0 v.u., was a possible site for Li. If the value were greater than 1.0 v.u., the Li would be too close to an O atom and if it were less than 1.0, the Li would be in a cavity where it would form bonds that would be too long. Moving the Li atom systematically through all points in the crystal gave a valence-sum map which revealed all the possible sites for Li.

In addition to finding the location of a particular type of atom, the valence-sum map reveals any unoccupied cavities in the structure including paths along which the atoms might easily diffuse. It is particularly useful for finding sites for interstitial atoms, making it a valuable tool for examining transport properties (Brown, 1988*a*).

An instructive way of displaying this map is to plot the valence-sum density map given by (13) where n is a number in the range 8 to 16.

$$f = \left(\frac{\sum_j s_{ij}}{V_i}\right)^{-n} \qquad (13)$$

This map has sharp peaks at minima in the valence map, *i.e.* at the positions of cavities in the structure, and falls off rapidly as the valence sum increases. The effect is to simulate an atomic density map around those atoms that fit snugly into the structure. Ideal atom sites have f equal to 1.0. Fig. 6 shows examples of Mg valence-sum density maps for forsterite (Mg_2SiO_4, Wenk & Raymond, 1973) plotted with $n = 16$ and $n = 8$.

Fig. 6(*a*) shows that there are two large cavities (indicated by shading). One is occupied by Mg(2) and the other is empty. In addition, at the origin is one well-matched site occupied by Mg(1) that correctly reflects the anisotropic motion. Setting n to 8 gives the map shown in Fig. 6(*b*). This gives an impression of the Mg positions expected at high temperature and shows the path along which the Mg(1) can diffuse using the empty site. The Mg(2) atom does not diffuse, nor does the center of the large cavity it occupies provide good bonding as the bonds are too long. The Mg(2) atom moves off center in its cavity by 0.08 Å, introducing a small steric distortion into the cation environment of the kind discussed in §4.

3.7. *Electronic distortions*

The equal-valence rule is often violated in cases where the cation environment is distorted by anisotropic electronic effects. The causes of the electronic distortions lie outside the scope of the bond-valence model but are well described in references such as Burdett (1980). In considering their influence on structure, electronic effects may usefully be classified according to the inherent strength of the distortion. Strong distortions, such as the lone-pair distortions found around As^{3+} or the Jahn–Teller distortion around Cu^{2+}, occur in all compounds regardless of the context in which the cation finds itself. All that needs to be determined is the extent and direction of

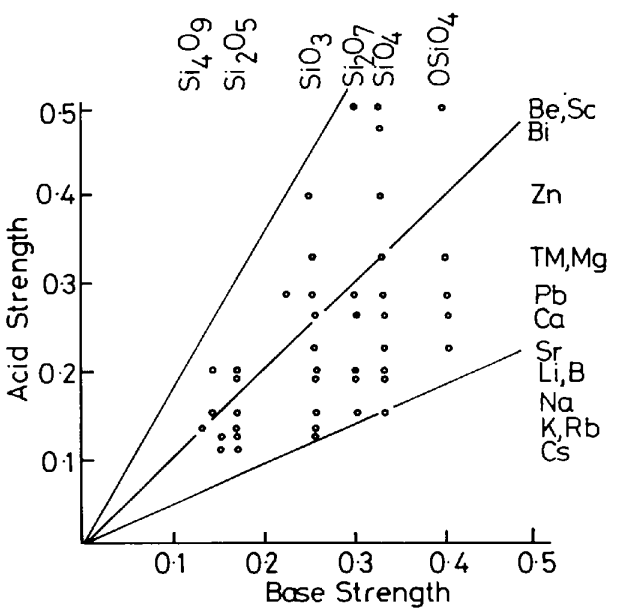

Fig. 5. Lewis acid strengths and Lewis base strengths of silicates illustrating the valence matching principle. TM = transition metal. The central line represents a perfect match. Circles indicate known stable silicates (Dent-Glasser, 1979).

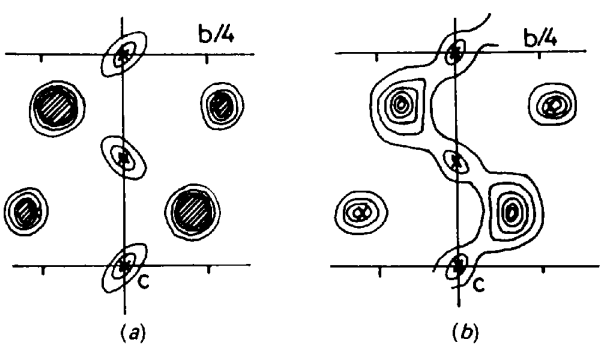

Fig. 6. Valence-sum density map for Mg atoms in forsterite calculated using equation (13) [reprinted with permission from Brown (1989), © 1989 American Chemical Society]. x indicates the position of Mg atoms. Contours are at intervals of 0.33. (*a*) Calculated with $n = 16$ giving the impression of Mg sites at room temperature. The shaded regions have values greater than 1.0 and represent cavities too large for Mg. (*b*) Calculated with $n = 8$ giving the impression of the sites at high temperature and revealing a diffusion path along the c axis.

the distortion, the latter necessarily being determined by the surrounding bond network. On the other hand, weak electronic distortions, such as those found around Tl^+ and Ti^{4+}, will only occur when the distortion is also predicted by the bond-network equations, (3) and (4), or required by steric constraints. For example, the size of the distortion around Tl^+ is determined by the Lewis base strengths of its ligands. If the bases are strong as in Tl_3BO_3 [$S_b(BO_3^{3+}) = 0.33$ v.u.] the bonds will be strong (0.33 v.u.) and the coordination number ($\simeq V/S_b$) small (3), forcing an sp^3 configuration with the lone pair occupying one of the orbitals. In this case the bonding will be strongly distorted. If the bases are weak as in $TlNO_3$ [$S_b(NO_3) = 0.11$ v.u.], the bonds will be weak and the coordination number large ($\simeq 10$) leaving no room for the lone pair. The result is a symmetric bonding environment for Tl^+ (Brown, 1988*b*). Ti^{4+} is usually found in regular octahedral coordination, but can be easily deformed by steric effects as in $BaTiO_3$ (see §4.3). In such cases, electronic effects help to stabilize distortions produced in other ways.

Cations that show electronic distortions are either low-oxidation state main-group elements or transition metals. The former constitute a well defined group whose cations form both strong and weak bonds. The properties of the strong bonds are well described by the valence shell electron pair repulsion (VSEPR) model (Gillespie & Hargittai, 1991) in which coordination sites not occupied by strong bonds are assumed to be occupied by lone electron pairs. The weak (or secondary) bonds (Alcock, 1972) are found close to, but not directly along, the directions occupied by the lone pairs. The distortion can be described as the cation moving off center in its coordination sphere and, according to the distortion theorem (§3.5.1), this will increase the average length of the bonds. As shown elsewhere (Brown, 1991*b*), it is this effect that makes it possible to introduce the small Bi^{3+} and Pb^{2+} ions into the superconductors $Bi_2Sr_2CuO_6$ (Michel, Hervieu, Borel, Grandin, Deslendes, Provost & Raveau, 1987) and $Pb_2Sr_2(Y,Ca)$-Cu_3O_8 (Marezio, Santoro, Capponi, Hewat, Cava & Beech, 1990).

Compared to the main-group elements, the electronic distortions of the transition elements are less systematic. The majority of transition metals have regular coordination and show no electronic distortions, but among those that do are V in higher oxidation states which typically forms one very strong bond to oxygen to give the vanadyl ion (VO^{n+}). Ti^{3+} and U behave somewhat similarly. Octahedrally coordinated Cu^{2+} almost always shows a tetragonal distortion that is attributed to the Jahn–Teller effect, the distortion removing the degeneracy in a partially occupied d^9 state (Dunitz & Orgel, 1957). The coinage metals in oxidation state 1+ and Hg^{2+} tend to form two strong linear bonds. The elements in the lower part of groups 11 and 12 are the classic 'soft' cations (Pearson, 1973), forming compounds in which the polarizability of the ions allows easy formation of electron-pair bonds with both 'soft' anions (*e.g.* S^{2-} and I^-) and 'soft' cations (as in Hg_2^{2+}).

In most cases electronic distortions violate the equal-valence rule but not the valence-sum rule. At best, such distortions are only qualitatively understood and it is not yet possible to predict quantitatively when and how they will occur. For this reason, electronically distorted structures will not be explicitly considered further in this work, though it should be kept in mind that electronic and steric effects often work symbiotically to stabilize distorted cation environments.

3.8. *Physical interpretations of bond valences*

Although bond valence, being an empirical concept, is completely defined by the assumptions made in §3.2, it is useful to ask how it relates to the more physical and traditional ideas of bonding. If atomic valence is defined to be equal to formal oxidation state (which is the most useful, but not the only possible, definition) it counts the number of valence electrons that an atom uses in bonding. Several physical interpretations are possible.

In the ionic limit, the atomic valence is the formal charge on an atom, the more electronegative atoms being the anions and the more electropositive the cations. The valence electrons of the cations are formally transferred to the anions where they form electron pairs with anion valence electrons to give closed-shell ions. In real compounds this transfer is never complete, the valence electron pairs being polarized back towards the cation. The bond valence is a simple extension of the electron-counting rules and gives a formal count of the number of electron pairs associated with the bonding region between the two ions. It does not itself indicate the degree of polarization of the electron pairs into the bonding region, and hence does not directly measure the covalency or the ionicity of a bond (but see the discussion below).

Because atomic valences are most easily interpreted as ionic charges, the bond-valence model has been perceived as a model applicable only to ionic solids. But bond valence can also be calculated starting with a covalent model. The simplest such model is the Lewis electron-pair-bond model in which bonds are represented as either electron-pair bonds (covalent) or electrostatic interactions (ionic). There are usually several Lewis structures for a given compound, and averaging over all them gives the number of electron pairs that correspond to a given bond, a

quantity that Boisson, Gibbs & Zhang (1988) call the resonance bond number. These are found to be close, or identical, to bond valences defined by (3) and (4) (Rutherford, 1991). Thus one gets the same value whether one starts from an ionic or covalent model. However, because of the correlation between Lewis acid strength and electronegativity (Brown & Skowron, 1990), the strong bonds formed by strong Lewis acids will tend to be more covalent, and the weak bonds formed by weak Lewis acids will tend to be more ionic. Bond valence, therefore, not only measures the number of electrons associated with a bond, but also, in practice, the degree of covalency (Brown & Shannon, 1973).

The bond-valence model can be compared with the two-atom-potential ionic model described in §2.3. The total binding energy in this model is given by summing the interatomic potentials (1) over all pairs of atoms. Consider first the Coulomb term. Its summation can be divided into two parts, an outer sum over the index i, and an inner sum over j. Consider a particular atom i. The contribution, U_i, of this atom to the total sum (the Madelung energy) is proportional to what Hoppe (1975) calls the MAPLE value (MAdelung Part of the Lattice Energy) and is given by (14).

$$U_i = \sum_j (Aq_iq_j/R_{ij}) \qquad (14)$$

This sum can be further divided into an infinite sequence of sums over the first, second, third, *etc.* neighbours. The contribution of each shell will have roughly the same magnitude as, but opposite sign to, the contributions of its two neighbouring shells. Thus the contribution of each shell will largely cancel half the contribution of the shell on either side, leaving U_i determined primarily by the contribution of the first coordination shell. The similarity between (6) and (14) with j restricted to nearest neighbours, suggests that U_i is related to the bond-valence sum around atom i, and that the constancy that Hoppe (1975) finds for the MAPLE value of a given cation in different structures is related to the valence-sum rule. O'Keeffe (1990) has also shown that the Madelung site potential, which is closely related to the MAPLE value, is, like the valence sum, proportional to the atomic valence.

At equilibrium, the derivative of the total energy with respect to R_{ij} must be zero. Using the Born–Landé potential (1), the equilibrium value of R_{ij} is given by (15).

$$2Aq_iq_j/NB = R_{ij}^{-(N-1)} \qquad (15)$$

A is a constant and if, following the arguments given by Brown & Shannon (1973), we assume B is proportional to the coordination number, $n = KB$, then (15) can be rewritten as (16).

$$q_i/n = (1/2AKq_j)R_{ij}^{-(N-1)} \qquad (16)$$

But q_i/n is equal to V_i/n which is just the expectation value of the bond valence (10) and, by comparison with (6), the bond-valence exponent, N', should be related to the Born exponent (N) by (17) as observed (Brown & Shannon, 1973).

$$N' = N - 1. \qquad (17)$$

In a similar way (5) can be related to either the Born–Mayer (2) (Jansen, Chandran & Block, 1991) or the Morse potential (Bürgi & Dunitz, 1987). Thus the form of the bond-valence curve is related to the form of the interatomic repulsion. All these analytical expressions for the repulsive potential are approximations valid over the short ranges of R_{ij} that are usually observed. Where the range is wider (*e.g.*, for H—O bonds) the true repulsion between two atoms is more accurately represented by a bond-length–bond-valence graph such as that shown in Fig. 2.

Bond valence can also be interpreted in terms of the matching of atomic surfaces. Bader (1990) has shown that the topology of the electron density can be used to divide space into unique atomic fragments that have special quantum-mechanical properties. The electron density found within a particular atomic fragment changes very little from one compound to another so that the problem of building a structure is the problem of assembling the atomic fragments. When the atoms are brought into contact, changes must be made at their boundaries to ensure the continuity of the electron density. Stable bonds will be formed when the electron densities at the bonding surfaces are already similar and only small adjustments are needed (*cf.* Miedema, Boom & De Boer, 1975). If one assumes that the Lewis acid and base strengths are related to the electron density at the surface of the atomic fragments, the valence-matching principle follows.

4. Steric effects

4.1. *Introduction*

The first corollary to the distortion theorem given in §3.5.1 predicts that the equal-valence rule will not be obeyed when an atom, usually a cation, is found in a cavity that is too large for it. Either the cavity will collapse around the atom or the atom will move off center. One would not expect this to be a common situation, since most compounds will select structures in which both of the network equations can be satisfied, but there are situations where the structure cannot exist without strain and where such distortion cannot be avoided. There are two principal causes of steric effects, local and non-local. Local steric effects arise when atoms are forced by local bonding requirements into contacts that are too

close. These are the steric effects found in organic molecules. Non-local steric effects arise from the constraints imposed by crystal symmetry, particularly translational symmetry which requires that all parts of a structure be commensurate. If the non-local steric effects produce too large a strain, the symmetry may be lowered or the structure may become incommensurate.

4.2. *Local steric effects: the hydrogen bond*

One of the most important and idiosyncratic linkages in chemistry is the hydrogen bond. The characteristic distortion found around the H atom is a local steric effect caused by hydrogen being too small for 2-coordination and too large for 1-coordination. Consider an H atom bonded to a single O atom. In a solid oxide the O atoms will be approximately close packed so that each O atom, including that bonded to H, will have several O neighbours about 3.2 Å away. Geometry requires that at least one of these must lie between 2.2 and 2.5 Å from the H atom as shown in Fig. 7(*a*).

An O atom at this distance from H forms a bond whose strength is between 0.08 and 0.05 v.u. (Fig. 2). The H atom cannot therefore be singly coordinated; there will always be at least one additional atom within bonding distance. According to the equal-valence rule, if the H atom is to be doubly coordinated, each bond should each have a valence of 0.5 v.u. corresponding to an H—O distance of 1.21 Å (Fig. 7*b*). This requires that the O atoms be only 2.42 Å apart, a distance at which they are strongly overlapping. Separating the O atoms until they are just in contact (3.2 Å), gives two symmetrical O—H bonds that are too long (1.6 Å) and a valence sum at H that is too small ($2 \times 0.25 = 0.50$ v.u.). According to the distortion theorem, the valence sums at H can be increased if the H atom goes off center, forming one long and one short O—H bond. With bonds of length 1.0 and 2.2 Å (0.9 and 0.1 v.u.) the O—O distance would be 3.2 Å and the valence sum at H would be 1.0 v.u. In practice, the O atoms are not hard spheres and two O atoms bonded to a common H atom will be brought closer together than 3.2 Å. Experimentally, it is found that equilibrium is reached when the O—H distances are 0.95 and 1.81 Å (0.83 and 0.17 v.u., Fig. 7*c*), the distances found in ice where the hydrogen bond is unperturbed by the presence of other elements (Brown, 1976*a*).

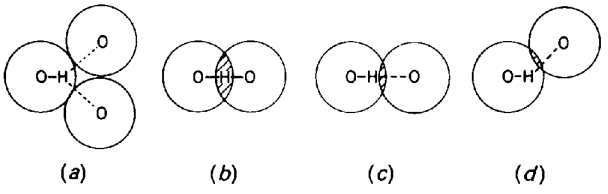

Fig. 7. Configurations of hydrogen bonds. The O atoms are shown as circles corresponding to a non-bonding distance of 3.2 Å. (*a*) A singly coordinated H atom is still within bonding range of other O atoms (H···O = 2.2 to 2.5 Å). (*b*) A symmetrical hydrogen bond causes the O atoms to overlap (O—O = 2.42 Å). (*c*) In a normal hydrogen bond the H atom is off-center (O—O = 2.76 Å). (*d*) Weak hydrogen bonds are usually bent.

The distortion occurs in such a way as to place the H atom closer to the stronger base, preferably a base with $S_b \geq 0.83$ v.u. If the donor O has a base strength much less than 0.83 v.u. [*e.g.* H_2O when H^+ is added to form H_3O^+, $S_m(O) = 0.4$ v.u.], or if the acceptor O has a base strength much greater than 0.17 v.u. (*e.g.* PO_4^{3-}, $S_b = 0.25$ v.u.), the H atom can be forced to form a more symmetric bond. In the monohydrated hydronium ion, $H_2O—H—OH_2^+$, the bond is completely symmetrical (Kjällman & Olovsson, 1972). On the other hand, if the acceptor has a base strength much less than 0.17 v.u. (*e.g.* ClO_4^-, $S_b = 0.08$ v.u.), the hydrogen bond will become weaker and more asymmetric. In this case, the hydrogen bond is free to bend and the O—H···O angle is found to deviate from 180° in such a way as to keep the O atoms at their effective contact distance as shown in Fig. 7(*d*) (Brown, 1976*a*,*b*).

Hydrogen bonds between other bases (F^-, Cl^-, Br^-, S^{2-}, N^{3-}, C^{4-}) behave in a similar way. Fluorine, being smaller than O, is able to form symmetric hydrogen bonds more readily (as, *e.g.*, in the FHF^- ion), but C—H···*X* hydrogen bonds are always highly asymmetric. In many molecules there is little or no excess valence (charge) associated with an H atom attached to C, but in a neutral molecule with an exposed Lewis base (*e.g.* O in CH_3CHO), the valence-sum rule requires that, if the O atom acts as a Lewis base, the H atoms must act as Lewis acids with the same total valence. Normally, the acid strength of H is small (less than 0.03 v.u.) but sufficient to produce a measurable interaction of the C—H group with a base (H···O ≃ 2.7 Å). In some cases, *e.g.* $CH_3C(OH)_2^+$, the Lewis acid strengths of the methyl H atoms may be as large as 0.1 v.u. In such cases the C—H···O bonds do not become stronger; the bonds individually remain weak but increase in number to three or four (Brown, 1980).

Because of its small size, H^+ always finds itself in a cavity that is too large and so, except in the most unusual circumstances, it forms an asymmetric link between two or more anions. Clearly such distortions are stabilized if these anions have base strengths close to the expected valences of the bonds.

4.3. *Non-local steric effects: distortions in perovskites*

Non-local steric effects arise from geometric constraints associated with symmetry, particularly trans-

lational symmetry. The cubic perovskites, ABO_3, contain two kinds of bond, A—O and B—O as shown in Fig. 8(*a*).

Since the A atoms are 12-coordinate, their bonds have valences $V_A/12$. The smaller B atoms usually have a larger atomic valence (V_B), are 6-coordinate, and have bonds of valence $V_B/6$. The B—O bonds are therefore much stronger than the A—O bonds. The structure can usefully be thought of as a strongly bonded framework of face-sharing cubes of composition BO_3 containing weakly bonded A atoms in the cube centers. In $BaTiO_3$ the network equations predict that the Ba—O (A—O) bond lengths should be 2.942 Å ($s = 0.17$ v.u.) and the Ti—O (B—O) bond lengths 1.965 Å ($s = 0.67$ v.u.). The Ba—O bonds require a lattice spacing of $a = 2^{1/2}$(Ba—O) = 4.161 Å while the Ti—O bonds require a lattice spacing of $a = 2$(Ti—O) = 3.930 Å. If the real structure has a lattice spacing equal to the average of these, 4.046 Å, the Ba—O bonds must be compressed and the Ti—O bonds stretched to yield a structure which violates the valence-sum rule, having a strain index, $R1$ [equation (8)] equal to 0.35 v.u. Ti finds itself in a cavity that is too large and tends to move off center in accordance with the first corollary of the distortion theorem (Fig. 8*b*). This distortion involves the loss of the center of symmetry and results in $BaTiO_3$ being a technologically important ferroelectric material. Other perovskites such as $PrFeO_3$ (Marezio, Remeika & Dernier, 1970) have the B (Fe) atom too large and the A (Pr) atom too small. In such compounds it is the environment of the A atom that distorts. The BO_3 framework twists, shortening some A—O bonds and lengthening others while keeping the average A—O distance constant (Fig. 8*c*). It is always the environment of the stretched atom that distorts, increasing its bond-valence sums in accordance with the distortion theorem.

The perovskite structure is the first member of a series of related compounds which includes the copper oxide superconductors. They are built from layers of composition AO and BO_2, the perovskite structure itself being produced by a simple alternation. In order to form crystals, the layers must be commensurate, that is, the ratio of the A—O to B—O bond lengths within the layers is constrained by the crystal structure to be equal to $2^{1/2}$. However, the ratio of the ideal bond lengths predicted by the network equations will, in general, be different. If the structure is to form at all, it will be strained, with one type of layer being stretched, the other compressed. Several mechanisms are available for relieving the stresses that produce this strain (Brown, 1991*b*).

(1) The first mechanism is always to relax the interlayer bonds in order to minimize the deviations from the valence-sum rule.

(2) The low valence sums that occur around cations in stretched layers can be increased by distorting their environment, a mechanism that is favoured if it can be stabilized by an electronic distortion of the cation's valence shell (§3.7). Fig. 9 shows how the lengths of Bi^{3+}—O bonds, and the corresponding lattice spacing of a BiO layer, change as Bi undergoes a trigonal off-center displacement in an octahedral coordination environment.

(3) In cases where the cations can exist in more than one oxidation state, the stress may be sufficient to move electrons from the compressed to the stretched cations stabilizing an otherwise unexpected oxidation state. Fig. 10 shows the changes expected

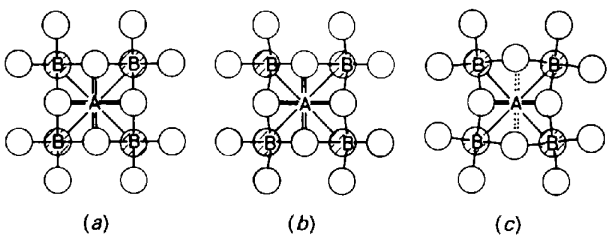

Fig. 8. Perovskite structures. The open circles are O atoms in the BO_2 layer, the shaded circles are O atoms in the AO layer behind. AO and BO_2 alternate. (*a*) The undistorted cubic structure. (*b*) The distortion found when the A—O bonds are compressed and the B—O bonds stretched (A too large, B too small). (*c*) The distortion found when the A—O bonds are stretched and the B—O bonds compressed (A too small, B too large).

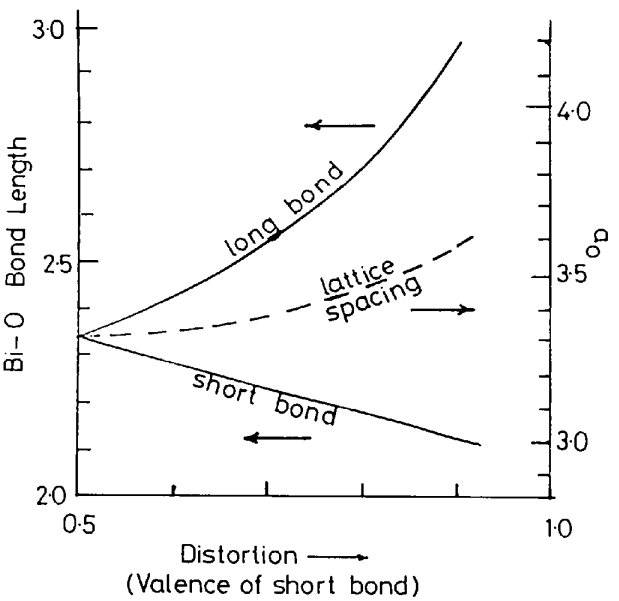

Fig. 9. The Bi^{3+}—O bond lengths in a trigonally distorted BiO_6 octahedron as a function of the degree of distortion. The right-hand scale shows the lattice spacing in BiO layers formed from the octahedra [reprinted with permission from Brown (1991*b*)].

in the lattice spacings of TlO and CuO_2 layers as charge is transferred between the cations. In the superconductor $Ba_2YCu_3O_7$, the strain is completely relieved by redistributing the charge between the two crystallographically distinct Cu atoms (Brown, 1991*a*).

(4) Buckling the compressed layers not only increases the bond length within the layer for a given lattice spacing, but distorts the environment of the cation in the adjacent stretched layer, both effects tending to reduce the strain index $R1$.

(5) The introduction of appropriate interstitial atoms or vacancies may not only relieve the stress in the neighbourhood of the defect, but may make beneficial changes in the oxidation states of other cations. The last two effects are illustrated by La_2NiO_4 discussed in §5.2.3.

These mechanisms all help to relieve the stress but usually at some cost in energy which can have an important influence on the properties of the solid. The cost of distorting the structure can often be reduced if the distortions lead to favourable electronic configurations.

4.4. *Residual bond strain in crystals*

Steric distortions necessarily violate the equal-valence rule but, if the stress cannot be completely relaxed, the valence-sum rule may also be violated. At room temperature, $R1$ may be as high as 0.2 v.u. and at elevated temperatures even higher values can be found. The strain associated with this violation of the valence-sum rule is referred to as the *residual bond strain*.

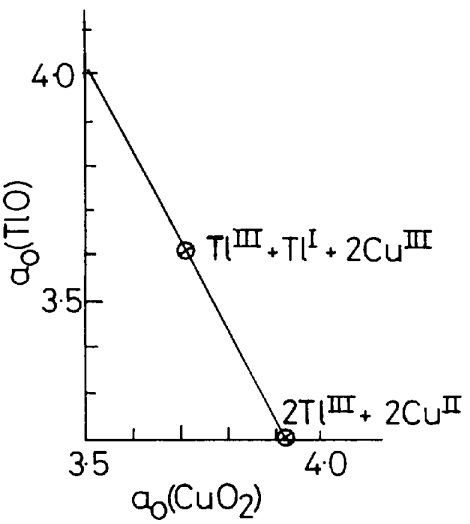

Fig. 10. The lattice spacing of a TlO layer as a function of that for a CuO_2 layer as charge is transferred from Cu to Tl. The two layers become commensurate at a lattice spacing of 3.69 Å with Cu in an oxidation state greater than 3+ (Brown, 1991*b*).

In some isomorphous series of structures, certain sites are found to be consistently under- or overbonded (bond-valence sums too small or too large) indicating the presence of tensile or comprehensive bond strain respectively. Wagner & O'Keeffe (1988) have shown that the Al(2) site in β-aluminas and magnetoplumbites is consistently underbonded (typically 2.7 rather than 3.0 v.u.), an effect they attribute to the local influence of repulsion between the Al atoms. Similar strains have been found in a number of other systems such as the melilite structures (Armbruster, Röthlisberger & Seifert, 1990), the perovskite-related Bi_3TiNbO_9 (Thompson, Rae, Withers & Craig, 1991) and La_2NiO_4 (Brown, 1991*c*). In all these studies, structures stable at room temperature had $R1 < 0.20$ v.u. Structures with $R1 > 0.20$ v.u. were found to be unstable and to relax in such a way as to reduce $R1$ below 0.20 v.u.*

Residual bond strain is indicated by experimental values of $R1$ that are too large to be attributed to experimental uncertainty and its presence can be expected to affect the physical properties of a crystal. In the copper oxide superconductors, the maximum superconducting transition temperature attainable by a particular structure appears to be related to the bond strain in the CuO_2 layers, transition temperatures above 90 K being associated with tensile, and lower transition temperatures with compressive, strain (Brown, 1990). The most general phenomenon associated with bond strain is the soft-mode transition, a phase transition that occurs when one of the vibrational modes of the crystal softens and freezes out, producing a distortion around an atom in tensile strain. As temperature is reduced in such materials, a sequence of collapsed structures appears each one having a lower symmetry and lower strain index than the one before.

5. Modelling inorganic crystal structures

5.1. *Strategies for modelling*

The relative influences of chemical and steric constraints are best understood when a crystal structure is generated from first principles. This section gives three examples of the use of the bond-valence model, illustrating the interplay of chemical and steric constraints. The goal of modelling is to predict the structure and geometry of a compound and hence its crystal chemistry, starting with only its chemical formula and such chemical and crystallographic knowledge as is implicit in the bond-valence model. The procedure can usefully be divided into three

* Although $R1$ never exceeds 0.20 v.u. in these three cases, there is no particular reason to assume that this limit will apply to all crystals. More work needs to be done to define the limiting value of $R1$ in crystals of different kinds.

steps, predicting the structure, *i.e.*, determining the bond network, determining the ideal bond lengths from the network, and mapping the structure into three dimensions.

The graph is constructed, as illustrated for $Mg_2CdCl_6.12H_2O$ in §5.2.1, by arranging the atoms of the chemical formula in a list in decreasing order of their Lewis acid or base strength. Bonds are first formed between the strongest Lewis acid and the strongest base. This generates a complex to which a Lewis base (or acid) strength is assigned. The complex is then inserted back into the ordered list at the appropriate place and the process is repeated until all bonds stronger than 0.2 v.u. have been formed. Bonds weaker than 0.2 v.u. are sensitive to the steric requirements of crystal packing and are best identified after the structure has been mapped into real space. One aid in constructing the bond graphs is the principle of maximum symmetry. At the stage where one knows only the chemical composition, all atoms of a given element are equivalent. As the graph is constructed, this equivalence is maintained as long as possible. This means that each cation will, as far as possible, form an equal number of bonds to every anion and *vice versa*.

When this stage is completed, the structure is represented by a finite graph which may, depending on whether there are unassigned weak bonds, consist of one or more independent complexes (see Figs. 11*a* and 13*a* for examples). If these complexes contain more than one bond between the same two atoms (as in Fig. 13*a* but not in Fig. 11*a*), it is likely that the real-space structure will be infinitely connected, thereby defining one or more lattice translations. Some of the atoms in the bond graph will have identical connectivities and so will be graphically equivalent. Wherever possible such atoms will also be related by crystallographic symmetry. For example, the graph shown in Fig. 13(*a*) has two O atoms labelled O(1) that are graphically equivalent and which, in the parent structure of the solid, are related by crystallographic symmetry. In favourable cases, the bond graph is sufficient to determine both the unit cell and the space group as discussed in the examples below.

Structures containing weak Lewis acids and bases may not, at this stage, be infinitely connected (see Fig. 11*a*). In such cases it is usually possible to treat a complex as a sphere (or some other simple shape) whose dimensions and symmetry can be predicted from the bond graph. For these compounds, the crystal structure is generated by considering the possible packings of the complexes (Brown & Duhlev, 1991). A valence-sum map (§3.6) may be useful in locating the sites occupied by alkali-metal atoms.

Once the structure has been mapped into three dimensions and the bond graph is complete, the network equations can be used to predict ideal bond lengths (making corrections for any expected electronic distortions). These are used to refine the atomic coordinates using, for example, a distance least-squares program such as *DLS* (Villiger, 1969). In most cases, the bond distances do not provide sufficient constraints to determine all the cell dimensions and atom coordinates, and non-bonded distances (or inter-bond angles) must also be supplied. Several methods of predicting non-bonding distances have been proposed, *e.g.*, relating them to valences of neighbouring bonds (Brown, 1987), minimizing their electrostatic repulsion (Pannetier, Bassas-Alsina, Rodriguez-Carvajal & Caignaert, 1990), or minimizing a short-range repulsion function (O'Keeffe, 1991). It is not yet clear which of these gives the best results, but the precise lengths are not critical since there are more than enough non-bonded distances and they are usually given low weight. This method can predict bond lengths to within 0.05 Å providing electronic and steric distortions are not present.

O'Keeffe (1991) has proposed an alternative approach in which the atomic coordinates are refined directly against the network equations. In this case, as with modelling by simulated annealing (Pannetier *et al.*, 1990), explicit information about the strain is lost because the bond geometry is constrained to exist in three-dimensional space. While these approaches show promise for predicting structure, they cannot be used to explore the influence of steric constraints.

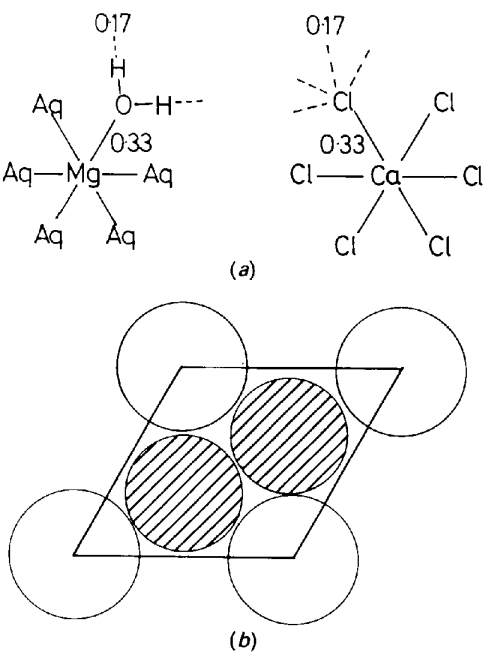

Fig. 11. The structure of $Mg_2CaCl_6.12H_2O$. (*a*) The bond graph. The numbers are the predicted bond valences. (*b*) Packing of the ions into layers.

Steric effects are necessarily present when the coordinate refinement is overdetermined, *i.e.*, when the number of free parameters in the model is less than the number of constraints provided by the network equations. In such cases it is not possible to find a set of coordinates that will exactly reproduce all the predicted bond lengths (*cf.* the case of cubic $BaTiO_3$, discussed in §4.3, where there are two bond lengths to be fitted by only one free parameter, the unit-cell length). In these cases least-squares fitting to the ideal bond lengths does not reproduce the observed atomic coordinates and it is necessary to explore the different ways in which the structure can relax. Examples are given below for $CaCrF_5$ (§5.2.2) and La_2NiO_4 (§5.2.3).

5.2. *Examples of modelling*

Three examples of modelling are given to illustrate the interplay of chemical and steric constraints. The first example, $Mg_2CaCl_6.12H_2O$, illustrates the way in which a bond graph is constructed to give two complexes which can be packed in different ways. The other two examples, $CaCrF_5$ and La_2NiO_4, have complete bond graphs and both can be mapped into three-dimensional tetragonal structures, but in neither case is the fit perfect. The highly strained tetragonal struture of $CaCrF_5$ requires changes so large that they change the bond graph itself. The new bond graph, corresponding to a monoclinic structure, gives good predictions of the bond lengths and hence the unit cell and atomic coordinates. The somewhat smaller stresses generated in tetragonal La_2NiO_4 can be relaxed by a variety of less drastic mechanisms, but these lead to an unusual crystal chemistry involving non-stoichiometry, oxidation of Ni, displacive phase transitions and residual bond strain.

5.2.1. $Mg_2CaCl_6.12H_2O$. This compound illustrates the sequence of steps needed to build the bond graph, and the way in which packing of discrete complexes can be used to determine the structure. The discussion follows that given by Brown & Duhlev (1991).

An ordered list of Lewis acid and base strengths of the atoms in the chemical formula is shown as the first line in Table 3.

At the second line bonds have been formed between H and O to form 12 water molecules. At the third line a complex has been formed by Mg. The choice of bonding Mg to H_2O rather than Cl is determined by the preference of the harder cation (Mg^{2+}) for the harder ligand (H_2O) and the softer cation (Ca^{2+}) for the softer ligand (Cl^-) (Balarew & Duhlev, 1984). At the fourth line the $CaCl_6^{4-}$ complex ion has been formed. The graph building then ends since only bonds weaker than 0.2 v.u. are left to be formed. The graph contains three spherical complexes, two of $Mg(H_2O)_6^{2+}$ and one of $CaCl_6^{4-}$ (Fig. 11*a*), whose effective radii have been shown by Brown & Duhlev (1991) to be 0.55 Å longer than the length of the metal–ligand bond.

Table 3. *Assembly of* $Mg_2CaCl_6.12H_2O$ *into complexes*

At each stage in the formation of the bond graph the Lewis acid strength (positive) or the Lewis base strength (negative) of the complex is given.

(1)	$24H^+$	$12O^{2-}$	$2Mg^{2+}$	Ca^{2+}	$6Cl^-$
	0.83	−0.50	0.33	0.27	−0.17
(2)	Bond 24H to 12O to form $12H_2O$				
	$2Mg^{2+}$	Ca^{2+}		$12H_2O$	$6Cl^-$
	0.33	0.27	0.17	−0.17	−0.17
(3)	Bond 2Mg to $12H_2O$ to form $2Mg(H_2O)_6^{2+}$				
	Ca^{2+}	$2Mg(H_2O)_6^{2+}$	6Cl		
	0.27	0.17	0.17		
(4)	Bond Ca to 6Cl to form $CaCl_6^{4-}$				
	$2Mg(H_2O)_6^{2+}$	$CaCl_6^{4-}$			
	0.17	0.17			
(5)	All further bonds are weaker than 0.2 v.u. and must be determined by crystal packing				

Cell constants for space group $R\bar{3}$

	Calculated	Observed (Clark, Evans & Erd, 1980)
a (Å)	10.14	10.24
c (Å)	17.32	17.12

The cation complex thus has a radius of 2.65 Å, the anion complex a radius of 3.26 Å, which gives a radius ratio of 0.81, corresponding to a cation coordination number beween 8 and 12. There are no simple packing structures that give cation coordination numbes as high as eight for a cation:anion ratio of 2:1. The highest possible cation coordination number is four which is found in the anti-fluorite structure observed, *e.g.*, for Na_2O. An ordered hydrogen-bonded scheme is possible in this arrangement in space group $F23$ with $a = 13.65$ Å and both ions on sites of 23 symmetry. Each cation has four anion nearest neighbours and six cation second-nearest neighbours only 15% further away. However, more densely packed structures with eight mixed anion and cation nearest neighbours are possible. The 2:1 stoichiometry lends itself to forming close-packed layers (Fig. 11*b*) which can stack in a two- or three-layer sequence in the space groups $P31c$ and $R\bar{3}$ respectively. Each complex lies on a threefold axis and is linked to its neighbour by an ordered hydrogen-bond array with each cation having, on average, four anion and four cation neighbours. The $F23$ structure has not been observed, but both the $P31c$ and $R\bar{3}$ structures are known for related compounds. $[Mg(H_2O)_6]_2CaCl_6$ itself crystallizes with the $R\bar{3}$ structure and the calculated and observed cell constants are in good agreement (Table 3). The valence-sum rule applied at Mg and O requires the H—Cl bonds to have a valence of only 0.17 v.u., *i.e.*, the atoms bonded to H require it to adopt the asymmetric configuration which best relieves the local steric stress.

This example shows that when the complex ions are linked only by weak bonds, several structures may be possible and frequently more than one is found. The problem yet to be tackled is to determine which will be the most stable.

5.2.2. $CaCrF_5$. $CaCrF_5$ is an example of a compound whose bond graph maps into an excessively strained structure in which the stress can only be removed by rearranging the graph.

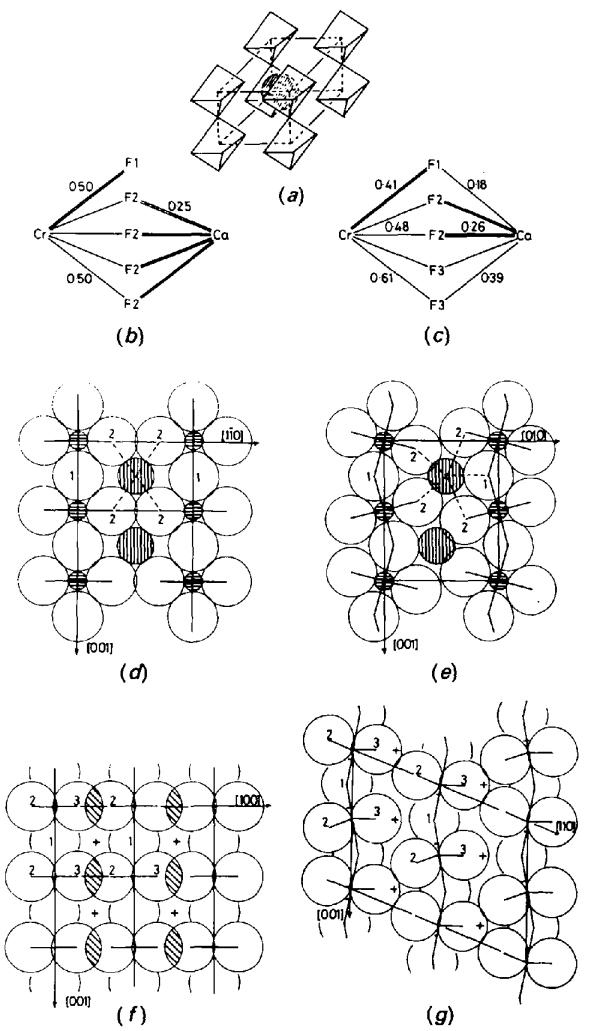

Fig. 12. The structure of $CaCrF_5$. (*a*) The mapping of (*b*) into a tetragonal structure. (*b*) The initial bond graph (tetragonal) showing predicted bond valences. (*c*) The modified bond graph after the structure relaxes (monoclinic) showing predicted bond valences. (*d*) View of the tetragonal structure in the plane (110) perpendicular to the axis of rotation of the CaF_6 octahedra. Plane circles are F, horizontally shaded circles are Cr and vertically shaded circles are Ca. (*e*) Same view as (*d*) after rotation (monoclinic structure). (*f*) View of the tetragonal structure down [010]. Regions where the F atoms overlap are shown with diagonal shading. + marks the position of Ca in adjacent layers. (*g*) Same view as (*f*) after shearing (monoclinic structure).

The Lewis acid strengths of Cr^{3+} and Ca^{2+} are 0.50 and 0.274 v.u. respectively, the Lewis base strength of F^- is 0.21 v.u. ($S_m = 0.5$ v.u.). Cr will therefore form six bonds of 0.5 v.u. to F, requiring one of the F atoms to be bonded to two Cr atoms (left-hand side of Fig. 12*b*).

The twice-bonded F(1) ensures that the CrF_5 complex will be infinitely connected in one direction, and establishes one of the lattice translations as 2[Cr—F(1)] = 3.82 Å. The polymeric CrF_5^{2-} complex can form bonds with valences ranging from $S_b = 0.5/3 = 0.17$ v.u. to $S_m = 0.5/1 = 0.50$ v.u. since each non-bridging F has 0.5 v.u. of unused valence and may form from one to three additional bonds. With a Lewis acid strength of 0.27 v.u., Ca will be 7- or 8-coordinate. Eight-coordinated Ca can form two bonds with each of the remaining four F atoms to give a graph in which all the Cr—F bonds have lengths of 1.913 Å ($s = 0.50$ v.u.) and all Ca—F bond lengths of 2.357 Å ($s = 0.25$ v.u.). Such a graph has fourfold symmetry around the Cr—F—Cr chain and

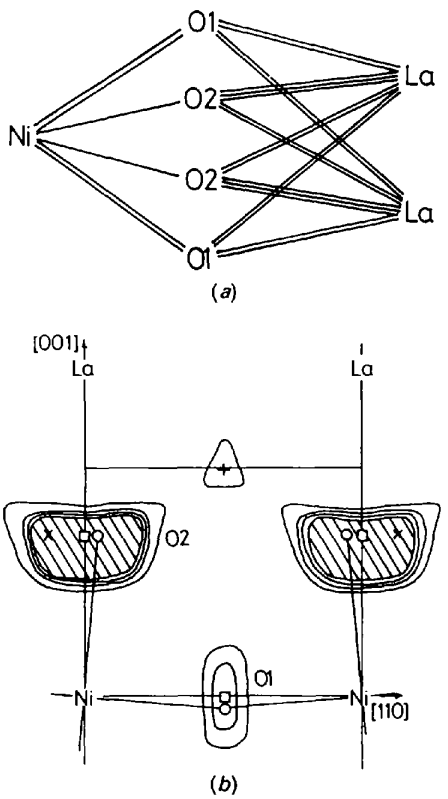

Fig. 13. The structure of La_2NiO_4. (*a*) The bond graph. All bonds have a predicted valence of 0.33 v.u. (*b*) Valence-sum density map for O in La_2NiO_4 calculated using equation (13) with $n = 16$. Cavities too large for unstrained O atoms are shaded. Squares show the positions of O in the tetragonal structure, circles show their position in the *Bmab* structure, + show the position of the interstitial and x the relaxed positions of the O atoms adjacent to the interstitial.

around Ca, and can be mapped into a cell in the tetragonal space group *P4/mmm* (Fig. 12*a*) with the *c* axis determined by the length of the Cr—F—Cr bridge and the *a* axis by both the Ca—F and Cr—F bond lengths ($a = 4.648$, $c = 3.826$ Å). However, this brings F atoms in adjacent chains much too close (1.94 Å, see the shaded region in Fig. 12*f*) and the structure has to relax. The first relaxation is a rotation of the linked CrF_6 octahedra about an equatorial Cr—F bond to provide better packing in the tetragonal (110) plane (Fig. 12*d* to 12*e*). Because the octahedra are linked through the shared F(1) atom, alternate octahedra along the chain must rotate in opposite directions, doubling the *c* axis. The rotation stops when the F(2) atoms on adjacent octahedra along the chain are just in contact (2.8 Å), but this is a large enough rotation to bring the bridging F(1) atom into the Ca coordination sphere. The second relaxation, a shearing along the *c* axis in the plane perpendicular to the rotation axis, is required to increase the very short F—F contacts (Fig. 12*f* to 12*g*). It removes two of the Ca—F(2) bonds, reducing the net Ca coordination from eight to seven when the new Ca—F(1) bond is included. In Table 4 the cell dimensions and bond lengths predicted from the new bond graph (Fig. 12*c*) are compared with those observed (Wu & Brown, 1973).

The relaxed structure has monoclinic symmetry, space group *C2/c* with Cr on a center of symmetry and Ca and F(1) on a twofold axis. The monoclinic cell dimensions are given by $a_m = x/\sin(\beta)$, $b_m = 2^{1/2}a_t$, $c_m = 2c_t$ and $\beta = \cos^{-1}(c_t/x)$ where $x = [\text{Cr—F(3)} + \text{Ca—F(3)}]$. Noteworthy is the fact that the two Ca—F(2) bonds, which are equivalent in the bond graph but which are required by the rotation of the octahedra to be different (see Fig. 12*e*), have a mean length which is exactly equal to the ideal length predicted using the network equations.

This structure illustrates how the effect of a large stress can result in a change in the bond graph, which allows for improved packing. The valence-sum rule is obeyed and, apart from small differences in the two graph-equivalent Ca—F(2) bonds, the strain is completely relaxed.

5.2.3. La_2NiO_4. La_2NiO_4 is an example of a moderately strained structure that can be relaxed by several mechanisms, none of them drastic but none able to remove all the strain. The discussion follows that given by Brown (1991*c*).

La and Ni have Lewis acid strengths of 0.35 and 0.34 v.u. respectively and both form an acceptable match with O ($S_b = 0.5$ v.u.). Ni is expected to be 6-coordinate and La 9-coordinate. The bond network (Fig. 13*a*) is generated using the principle of maximum symmetry by forming six bonds from Ni to the four O atoms (two bonded once and two bonded twice) and nine bonds from each La (two to each of the four O atoms with an additional bond to one of the underbonded O atoms). The equivalence of the two La atoms in the formula is preserved, but the four O atoms are divided into two groups [O(1) and O(2)] with different connectivities.

Table 4. *Calculated and observed distances* (Å) *in* $CaCrF_5$

	Calculated	Observed (Wu & Brown, 1973)
Tetragonal structure *P4/mmm*		
a (Å)	4.648	Not known
c (Å)	3.826	
Cr—F	1.913	
Ca—F	2.357	
Monoclinic structure *C2/c*		
a (Å)	9.517	9.005
b (Å)	6.573	6.472
c (Å)	7.652	7.533
β (°)	118.3	115.8
Cr—F(1)	1.989	1.940
Cr—F(2)	1.927	1.918
Cr—F(3)	1.839	1.848
Ca—F(1)	2.476	2.495
Ca—F(2)	2.342	2.291, 2.391
Ca—F(3)	2.191	2.214

R.m.s. deviation = 0.04 Å [0.02 Å taking the mean of Ca—F(2) bonds].

This network exactly obeys both network equations with all bonds having an ideal valence of 0.33 v.u. corresponding to bond lengths of 2.57 and 2.06 Å for the La—O and Ni—O bonds respectively.

The large number of atoms joined by two or more bonds in Fig. 13(*a*) ensures that the structure will be infinitely connected in all three directions. Although it is not immediately obvious, the bond graph can be mapped into a structure with fourfold symmetry: the Ni—O(2) and one of the La—O(2) bonds can be placed along a fourfold axis and all the other bonds around Ni, O(2) and La occur four (or eight) times in the graph. The structure can be mapped *via* the square layers shown in Fig. 14(*a*), into a tetragonal cell in space group *P4/mmm*, giving five crystallographically distinct bonds and four degrees of freedom {*a*, *c*, *z*(La) and *z*[O(2)]} (Fig. 14*b*). The symmetry of the graph is preserved in the symmetry of the crystal except that in the crystal the La—O(2) bond that lies along the fourfold axis is not symmetry related to the other four.

This structure is necessarily strained since it is not possible to choose the four parameters to satisfy the all five predicted bond lengths. The ratio of the ideal La—O and Ni—O distances is 1.25, well below the 1.41 required by the crystal geometry. Consequently the La—O bonds within the layers must be stretched and the Ni—O bonds compressed leading to a breakdown of the valence-sum rule. The extent of this breakdown is indicated by *R*1 being equal to 0.47 v.u., much larger than the 0.2 v.u. limit often found for room-temperature stable compounds.

The first line of relaxation is to change the interlayer spacing. In principle, *R*1 could be reduced to

zero by moving O(2) 0.5 Å away from Ni towards La, but this produces an unacceptably large distortion around O(2). In practice the relaxation stops when $R1 = 0.27$ v.u. leaving the Ni atom in a tetragonally distorted environment similar to that caused by the Jahn–Teller effect in Cu^{2+}. In this relaxed structure, the NiO_2 layers are still compressed and the LaO layers still in tension. Further relaxation can be provided by buckling the NiO_2 layer which increases the Ni—O bond length and distorts the environment around La, both effects relieving the strain. Two forms of buckling are possible, leading to structures in the space groups, *Bmab* and $P4_2/ncm$ (Aleksandrov, 1987). The *Bmab* distortion provides greater relief of the strain for a given degree of buckling, but it also creates a larger distortion of the environment around O(2). Rotation of the NiO_6 octahedra by 6° reduces $R1$ to 0.20 but any further rotation again produces an unacceptably large distortion at O(2). This is the structure found at room temperature for La_2NiO_4 when prepared in vacuum. Further rotation of the octahedra can only occur in the $P4_2/ncm$ structure which is observed below 100 K.

When La_2NiO_4 is annealed in the presence of oxygen, it can take up interstitial O^{2-} since each interstitial O^{2-} ion increases the average charge of the Ni atoms and helps to fill out the LaO layers in its neighbourhood. Possible sites for the interstitial can be found using the oxygen valence-sum density map shown in Fig. 13(*b*). Three crystallographically distinct peaks can be seen in the map. The largest (shaded) corresponds to the large cavity occupied by O(2) in the stretched LaO layer. The next peak, corresponding to the O(1) site in the NiO_2 layer, is smaller than expected, consistent with the NiO_2 layers being compressed. The third and smallest peak lies between the two LaO layers and represents the best location for the interstitial O atom.

The optimum relief of both the tensile and compressive stress occurs when there is one interstitial per five or six formula units. At this concentration the oxidation state of Ni just equals its valence sum (2.3 v.u.) and all parts of the LaO layer are close enough to an interstitial to have their stress relieved. Fig. 15(*a*) shows a possible superstructure for $La_2NiO_{4.17}$ in which $R1 = 0.18$ v.u.

A different form of relaxation occurs in materials prepared with a La deficiency. Such compounds appear to contain LaO^+ vacancies, allowing the LaO layers to stretch (Choisnet, Bassat, Pilliere & Odier, 1988). A possible defect structure that satisfies the valence-sum rule is shown in Fig. 15(*b*). Thus either

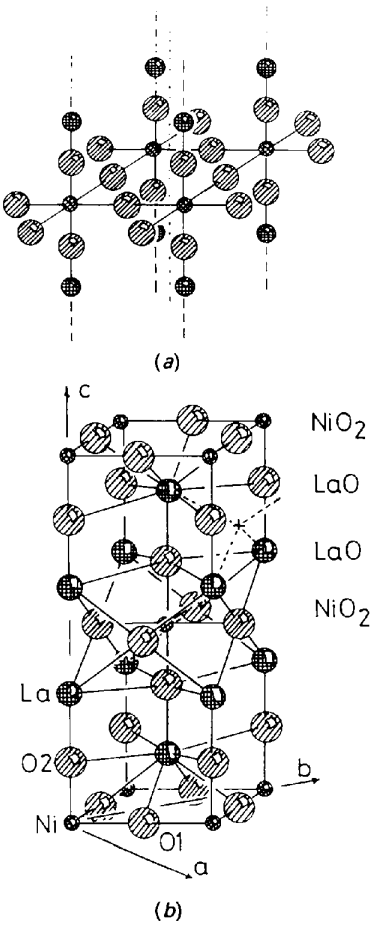

Fig. 14. The structure of La_2NiO_4. La atoms are vertically cross hatched, Ni atoms diagonally cross hatched. (*a*) The mapping of the bond graph into layers. In order of increasing size the circles represent Ni, La and O. (*b*) The stacking of layers to form the tetragonal parent structure.

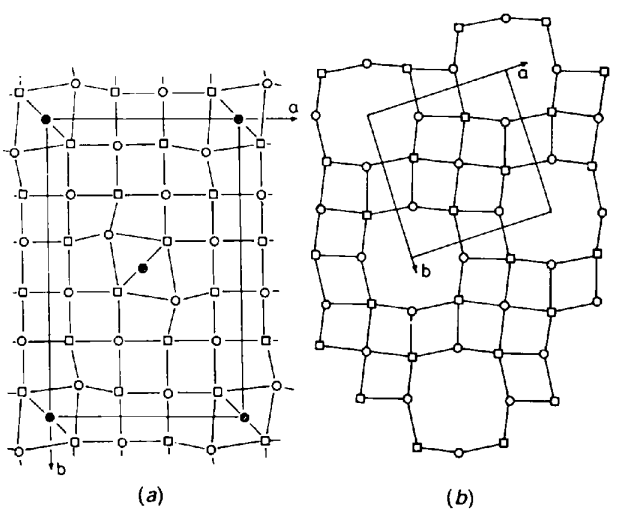

Fig. 15. Models of the LaO layers in defect structures of La_2NiO_4. Squares are La, circles are O. (*a*) 3 × 2 superstructure incorporating an interstitial O. The interstitial atom (shaded) lies between two LaO layers. (*b*) 5 × superstructure incorporating LaO vacancies. An La atom is missing from the layer shown and an O from the same position in the layer below.

adding interstitial O^{2-} or introducing LaO^{+} vacancies can relieve the stress within the LaO layer and simultaneously increases the oxidation state of Ni, relieving the stress in the NiO_2 layer as well.

The model predicts that La-deficient La_2NiO_4 should have an oxygen-deficient structure, and that material that is not La deficient will absorb about 0.2 interstitial O atoms per formula unit. If prepared in the absence of oxygen, the stoichiometric tetragonal structure, stable at high temperature, will undergo a displacive transition to a structure in space group *Bmab* and possibly, at lower temperatures, to one in $P4_2/ncm$.

La_2NiO_4 provides an excellent example of a compound in which the steric and chemical constraints are of equal importance. Relief of the steric stress is predicted to produce a tetragonal distortion in the environment of the Ni atom, to lead to an excess or deficiency of O in such a way as to stabilize Ni^{3+}, or to lead to a displacive phase transition that will give irregular La coordination. Using the bond-valence model, all these properties can be deduced from the chemical formula alone.

6. Concluding remarks

This article has explored the relationship between chemical and steric constraints in inorganic solids. The bond-valence model, which is described in some detail in §3, is an appropriate vehicle for such a study, as it allows the predicted bonding geometry of a compound to be compared with the geometries that are possible when the structure is mapped into three-dimensional space.

Three regimes are identified. When the bonds are strong, strain is not possible. Strained structures do not exist and the bonding geometry corresponds to that predicted by the bond-valence model. When the bonds are weak, they are often strained to accommodate the spatial requirements, but, because large strains correspond to only small changes in bond valence, the bond-valence rules are still obeyed. Between these two regimes is one where both chemical and spatial constraints are important. Large strains can be expected, but only those whose deviation from the valence-sum rule corresponds to $R1$ less than about 0.2 v.u. are stable at room temperature. In other cases the stresses can be reduced by either large or small changes in the structure. In particular, they can lead to non-stoichiometry, collapsed structures with lower symmetry and stabilization of unusual oxidation states. Many of the interesting properties of inorganic solids (*e.g.*, ferroelectricity and superconductivity) are related to steric strain. In particular, the tetragonal distortion found in the environment of the Ni atom in La_2NiO_4, the distortion that proved so perpelexing to those who carefully refined its structure, is seen to be a predictable consequence of the compression to which the NiO_2 layers are subject in order to be commensurate with the LaO layers.

I wish to thank the Natural Science and Engineering Council of Canada for financial support and Drs Daniel Altermatt, Rumen Duhlev, Anna Skowron, Hannah Dabkowska and other coworkers for stimulating discussions.

References

ALCOCK, N. W. (1972). *Adv. Nucl. Radiochem.* **15**, 1–58.

ALEKSANDROV, K. S. (1987). *Kristallografiya*, **32**, 937–950.

ARMBRUSTER, T., RÖTHLISBERGER, F. & SEIFERT, F. (1990). *Am. Mineral.* **75**, 847–858.

BADER, R. W. F. (1990). *Atoms in Molecules: a Quantum Theory*, International Series of Monographs on Chemistry 22. Oxford: Clarendon Press.

BALAREW, CHR. & DUHLEV, R. (1984). *J. Solid State Chem.* **55**, 1–6.

BERTAUT, F. (1952). *J. Phys. Rad.* **13**, 499–505.

BOBINSKI, W. & ZIOŁKOWSKI, J. (1991). *J. Solid State Chem.* **91**, 82–97.

BOISSON, M. B., GIBBS, G. V. & ZHANG, Z. G. (1988). *Phys. Chem. Mineral.* **15**, 409–415.

BORN, M. & LANDÉ, A. (1918). *Sitzungsber. Preuss. Akad. Wiss. Berlin*, **45**, 1048–1068.

BORN, M. & MAYER, J. E. (1932). *Z. Phys.* **75**, 1–18.

BRESE, N. E. & O'KEEFFE, M. (1991). *Acta Cryst.* **B47**, 192–197.

BROWN, I. D. (1976*a*). *Acta Cryst.* **A32**, 24–31.

BROWN, I. D. (1976*b*). *Acta Cryst.* **A32**, 786–792.

BROWN, I. D. (1977). *Acta Cryst.* **B33**, 1305–1310.

BROWN, I. D. (1980). *J. Chem. Soc. Dalton Trans.* pp. 1118–1123.

BROWN, I. D. (1987). *Chem. Phys. Mineral.* **15**, 30–34.

BROWN, I. D. (1988*a*). *Solid State Ionics*, **31**, 203–208.

BROWN, I. D. (1988*b*). *Acta Cryst.* **B44**, 545–553.

BROWN, I. D. (1989). *J. Chem. Inf. Comput. Sci.* **29**, 266–271.

BROWN, I. D. (1990). *Physica C*, **169**, 105–106.

BROWN, I. D. (1991*a*). *J. Solid State Chem.* **90**, 155–167.

BROWN, I. D. (1991*b*). *Chemistry of Electronic Ceramic Materials*, NIST Special Publication 804, edited by P. K. DAVIES & R. S. ROTH, pp. 471–483. Washington: National Institute of Standards and Technology.

BROWN, I. D. (1991*c*). *Z. Kristallogr.* **199**, 255–272.

BROWN, I. D. & ALTERMATT, D. (1985). *Acta Cryst.* **B41**, 244–247.

BROWN, I. D. & DUHLEV, R. (1991). *J. Solid State Chem.* **95**, 51–63.

BROWN, I. D. & SHANNON, R. D. (1973). *Acta Cryst.* **A29**, 266–282.

BROWN, I. D. & SKOWRON, A. (1990). *J. Am. Chem. Soc.* **112**, 3401–3403.

BURDETT, J. K. (1980). *Molecular Shapes*. New York: John Wiley.

BÜRGI, H.-B. & DUNITZ, J. D. (1987). *J. Am. Chem. Soc.* **109**, 2924–2926.

BURNHAM, C. W. (1990). *Am. Mineral.* **75**, 443–463.

BYSTRÖM, A. & WILHELMI, K. A. (1951). *Acta Chem. Scand.* **5**, 1003–1010.

CATLOW, C. R. A. (1977). *Proc. R. Soc. London Ser. A*, **353**, 533–561.

CATLOW, C. R. A., THOMAS, J. M., PARKER, S. C. & JEFFERSON, D. A. (1982). *Nature (London)*, **295**, 658–662.

CHOISNET, J., BASSAT, J. M., PILLIERE, H. & ODIER, P. (1988). *Solid State Commun.* **66**, 1245–1249.

CLARK, J. R., EVANS JR, H. T. & ERD, R. C. (1980). *Acta Cryst.* **B36**, 2736–2741.

DENT-GLASSER, L. (1979). *Z. Kristallogr.* **149**, 291–325.
DONNAY, G. & ALLMAN, R. (1970). *Am. Mineral.* **55**, 1003–1015.
DUNITZ, J. D. & ORGEL, L. E. (1957). *Nature (London)*, **179**, 462–465.
EWALD, P. P. (1921). *Ann. Phys. (Leipzig)*, **64**, 253–287.
GILLESPIE, R. J. & HARGITTAI, I. (1991). *The VESPR Model of Molecular Geometry*. New York: Prentice Hall.
HAWTHORNE, F. C. (1985). *Am. Mineral.* **70**, 455–473.
HAZEN, R. M. & PREWITT, C. T. (1977). *Am. Mineral.* **62**, 309–315.
HOPPE, R. (1975). *Crystal Structure and Chemical Bonding in Inorganic Chemistry*, edited by C. J. M. ROOYMANS & A. RABENAU, ch. 9, pp. 127–169. Amsterdam: North Holland.
JANSEN, L., CHANDRAN, L. & BLOCK, R. (1991). *J. Mol. Struct.* Submitted.
KHAN, A. A. (1976). *Acta Cryst.* A**32**, 11–16.
KJÄLLMAN, T. & OLOVSSON, I. (1972). *Acta Cryst.* B**28**, 1692–1697.
KRAMER, G. J., FARRAGHER, N. P., VAN BEEST, B. W. H. & VAN SANTEN, R. A. (1991). *Phys. Rev. B*, **43**, 5068–5080.
MAREZIO, M., REMEIKA, J. P. & DERNIER, P. D. (1970). *Acta Cryst.* B**26**, 2008–2022.
MAREZIO, M., SANTORO, A., CAPPONI, J. J., HEWAT, E. A., CAVA, R. J. & BEECH, F. (1990). *Physica C*, **169**, 401–412.
MICHEL, C., HERVIEU, M., BOREL, M. M., GRANDIN, A., DESLENDES, F., PROVOST, J. & RAVEAU, B. (1987). *Z. Phys. B*, **68**, 421–423.
MIEDEMA, A. R., BOOM, R. & DE BOER, F. R. (1975). *Crystal Structure and Chemical Bonding in Inorganic Chemistry*, edited by C. J. M. ROOYMANS & A. RABENAU, ch. 10, pp. 163–196. Amsterdam: North Holland.
MÜLLER-BUSCHBAUM, H. & LEHMANN, U. (1978). *Z. Anorg. Allg. Chem.* **447**, 47–52.
O'KEEFFE, M. (1989). *Struct. Bonding (Berlin)*, **71**, 161–190.
O'KEEFFE, M. (1990). *J. Solid State Chem.* **85**, 108–116.
O'KEEFFE, M. (1991). *Chemistry of Electronic Ceramic Materials*, NIST Special Publication 804, edited by P. K. DAVIES & R. S. ROTH, pp. 485–496. Washington: National Institute of Standards and Technology.
O'KEEFFE, M. & BRESE, N. F. (1991). *J. Am. Chem. Soc.* **113**, 3226–3229.
PANNETIER, J., BASSAS-ALSINA, J., RODRIGUEZ-CARVAJAL, J. & CAIGNAERT, V. (1990). *Nature (London)*, **346**, 343–345.
PAULING, L. (1927). *J. Am. Chem. Soc.* **49**, 765–790.
PAULING, L. (1929). *J. Am. Chem. Soc.* **51**, 1010–1026.
PEARSON, R. G. (1973). Editor. *Hard and Soft Acids and Bases*. Stroudsburg, PA: Dowden, Hutchinson & Ross.
RUTHERFORD, J. S. (1990). *Acta Cryst.* B**46**, 289–292.
RUTHERFORD, J. S. (1991). Private communication.
THOMPSON, J. G., RAE, A. D., WITHERS, R. L. & CRAIG, D. C. (1991). *Acta Cryst.* B**47**, 174–180.
VILLIGER, H. (1969). *DLS Manual*. Institut für Kristallographie und Petrographie, ETH, Zürich, Switzerland.
WAGNER, T. R. & O'KEEFFE, M. (1988). *J. Solid State Chem.* **73**, 211–216.
WALTERSSON, K. (1978). *Acta Cryst.* A**34**, 901–905.
WENK, H. R. & RAYMOND, K. N. (1973). *Z. Kristallogr.* **137**, 86–105.
WU, K. K. & BROWN, I. D. (1973). *Mater. Res. Bull.* **8**, 593–598.
ZACHARIASEN, W. H. (1954). *Acta Cryst.* **7**, 795–799.
ZIOLKOWSKI, J. & DZIEMBAJ, L. (1985). *J. Solid State Chem.* **57**, 291–299.

Acta Cryst. (1992). B**48**, 572–577

High-Pressure Phases in the System W–O. I. Structure of $WO_{1.09}$ by HRTEM

BY YU. A. BARABANENKOV, N. D. ZAKHAROV AND I. P. ZIBROV

Institute of Crystallography, Academy of Sciences of Russia, Leninsky prospekt 59, Moscow, Russia

V. P. FILONENKO

Institute of High Pressure Physics, Academy of Sciences of Russia, Troitsk, Moscow Region, Russia

AND P. WERNER

Institute of Solid State Physics and Electron Microscopy, Halle/Saale, Germany

(*Received* 25 *March* 1991; *accepted* 15 *November* 1991)

Abstract

A new type of tungsten oxide was synthesized from a mixture of W and WO_3 by a solid-phase sintering method under high-pressure conditions. The crystal structure of the new oxide $WO_{1.09}$ was investigated by selected-area electron diffraction and high-resolution transmission electron microscopy (HRTEM). It has the following unit-cell parameters: $a = 17.16$, $b = 10.32$, $c = 3.78$ Å, $V = 669$ Å^3, $Z = 44$, $\rho = 21\ (3)$ g cm^{-3}, and belongs to the space group $Cmm2$. The W positions were determined from computer-processed HRTEM structure images. The R-factor minimization procedure was used to refine cationic sites; $R' = 14.5\%$. It is shown that the crystal structure is formed by edge sharing WO_3 octahedrally and tetrahedrally coordinated W cations.

Introduction

High-resolution transmission electron microscopy (HRTEM) provides a unique possibility of investigating the structure of very small crystal fragments of about several hundred ångstroms in size. This size

0108-7681/92/050572-06$06.00